33RD CONGRESS
OF THE INTERNATIONAL COUNCIL
OF THE AERONAUTICAL SCIENCES
STOCKHOLM, SWEDEN, 4-9 SEPTEMBER, 2022

ICAS 2022 SWEDEN

EXPERIMENTS TO INVESTIGATE LIFT PRODUCTION MECHANISMS ON OSCILLATING TRAILING-EDGE FLAPS

Bremm, Martin[1], Hörnschemeyer, Ralf[1] & Stumpf, Eike[1]

[1]Institute of Aerospace Systems, RWTH Aachen Wuellnerstr. 7, 52062 Aachen, Germany

Abstract

In the work presented in this paper, we investigated the lift coefficient and the flow fields of an oscillating trailing-edge flap of a rigid aerofoil to gain insight in the involved unsteady aerodynamic phenomena leading to a substantial lift increase compared to the non-oscillating flap. The time-averaged lift coefficients show an increase of up to 71% and the lift peak occurs at a constant reduced frequency for all investigated oscillation amplitudes. Based on the literature and the experimental results an approach to explain the peak frequency of the lift coefficients is given.

Keywords: unsteady aerodynamics, oscillating flap, lift enhancement

1. Introduction

Various applications of a trailing-edge flap as an unsteady aerodynamic control device are described in the literature; e.g. for gust load alleviation [1], [2], suppression of transonic buffet [3], [4], and control of large negative pitch moments on helicopter rotor blades [6], [5], [7]. In addition, another application of a trailing-edge flap in unsteady operation is to increase the mean value of lift coefficient above the steady lift coefficient. This application is also described in the literature and is further investigated in this paper. The effect of a periodically oscillating trailing-edge flap is described by Greenhalgh [8], who also filed a patent for such lift-enhancement device [9]. In both cases, when used as a control device or as a lift enhancement device, a proper understanding of the aerodynamic phenomena is mandatory.

While steady aerodynamic phenomena are well understood, unsteady aerodynamic phenomena are still a topic of ongoing research. It was stated by Stevens and Babinsky [10] that despite the insight from early studies in the 1930th and in recent years there is still a lack of knowledge of the fundamental lift-producing mechanisms for high incidence pitch motions with separated flow fields. A simple pitching flat plate was investigated by Stevens and Babinsky to fill this lack of knowledge and give insight in the contribution of circulatory or non-circulatory mechanisms. During the acceleration phase of the flat plate, an additional effect contribute to the lift generation. A mass of fluid is accelerated creating an inertial reaction force. This effect is referred to as 'added mass' or 'virtual mass' contributing to the non-circulatory lift. While the circulatory lift lags behind in phase, the non-circulatory lift is not phase-shifted [11].

The aerodynamic phenomena of unsteady lift generation are mostly studied in the simple case of a purely translating or a pitching motion. The work presented here aims to describe the lift-producing mechanisms of a rigid aerofoil with an oscillating trailing-edge flap. A mathematical model of the unsteady lift of an aerofoil with an oscillating trailing-edge flap is given by Leishman, who extended Theodorsens function for a thin rigid aerofoil undergoing oscillatory heaving or pitching motions in incompressible flow [12]. Leishmans model relies on the assumptions of a thin flapped aerofoil and small angles of the oscillation amplitude. This limits the application of this model. The unsteady lift of a rigid aerofoil with an oscillating trailing-edge flap was investigated in wind tunnel experiments [13]. The effect of increasing lift coefficient with increasing frequency is well documented in the literature [14]. However, from those experiments it is still unknown, whether the lift increase is due

to a reattachment of the boundary layer, due to downstream-shift of the location of boundary layer separation or maybe attributed to third phenomenon. Within the cited experiments the lift increase was measured for a high angle of attack of 10° and no flow visualisation or flow field measurements are reported. Previous work of the authors of the present paper gave insight [15]: Although the boundary layer separation at the main wing in a test setup similar to those found in the literature is slightly shifted downstream with an oscillating trailing-edge flap, it was shown that the lift increases in both cases with and without a separated boundary layer. This showed that a reattached boundary layer or a shifted boundary layer separation is at least not the only reason for an increase of the mean lift coefficient.
In the present paper, we investigate the lift coefficient and the flow field of an oscillating trailing-edge flap of a rigid aerofoil to contribute to the answer which lift-producing mechanisms cause the total lift increase. For this purpose, a rigid aerofoil equipped with a trailing-edge flap capable of oscillating flapping motions is studied experimentally. By means of a parameter study, the lift forces are determined for different oscillation frequencies and the flow fields in the wake of the trailing edge flap are measured for specific cases.

2. Experimental Setup

2.1 Flow Facility

The experiments were conducted in a closed-circuit water tunnel (figure 1) with a test section length of 1.2 m, a cross-section of 0.54 m x 0.54 m and a characteristic turbulence level of 2 % - 3 %. The nozzle has a contraction ratio of 1.85; flow speeds range from creeping flow to 4 m/s. All experiments of this study are conducted at a chord-based Reynolds number of Re_c = 0.3x10^6, with the water temperature at 40 °C and the freestream velocity set to 1.32 m/s. The position of the aerofoil in the test section is indicated in figure 1 with the coordinate system (x, z).

2.2 Test Model

The test model is identical to the geometry used in [15]. Its aspect ratio Λ is 3 and the chord c has a length of 150 mm. The wing was manufactured of an aluminium alloy with high stiffness, to avoid bending. The two-dimensional geometry of the test model is sketched in figure 2. The test model with a NACA 2412 aerofoil has a plain flap hinged at 80 %. The gap of the plain flap between the main wing and the flap is 0.5 mm. As it can be seen in figure 2, $\bar{\eta}$ is the mean flap angle, $\hat{\eta}$ is the flap oscillation amplitude and the distance s is the stroke height of the oscillating trailing edge. To guarantee a fully turbulent boundary layer, transition trips of distributed roughness are applied close to the main wing leading edge on the top and on the bottom side. The laminar-turbulent transition correlates with the Reynolds number Re_h based on the height of the transition trip with roughness elements between 200 µm and 355 µm. The laminar-turbulent transition at Re_h = 600 was experimentally proven by Braun [16].

2.3 Balance Measurements

Figure 3 shows the experimental setup of the conducted experiments. The lower parts, i.e. the split plates, the wing and the wing mounts, are immersed in the test section below the water level. The upper parts, i.e. the balance, the electric motor and the flap kinematics are above the water level. The split plates are used on both sides of the wing, with a distance between the wing and the split plates of 0.1 mm. This allows balance measurements with low three-dimensional effects. The balance is positioned between the wing mount and the frame which is connected to the water tunnel. The origin of the coordinate system of the force balance (F_x, F_z, M_y) and the origin of the aerodynamic coordinate system (L, D, M) on mid-span position on the quarter-chord of the aerofoil are indicated in figure 3.
The balance ME-Meßsysteme K6D110 measures all six force and moment components. It is paired with a Q.brixx X station B data acquisition unit with three Q.brixx XL A101 transducer modules. The six components from the balance are recorded with an acquisition frequency of 20 kHz. The data acquisition unit also records the temperature and the flap deflection angle and synchronises all measurement signals.

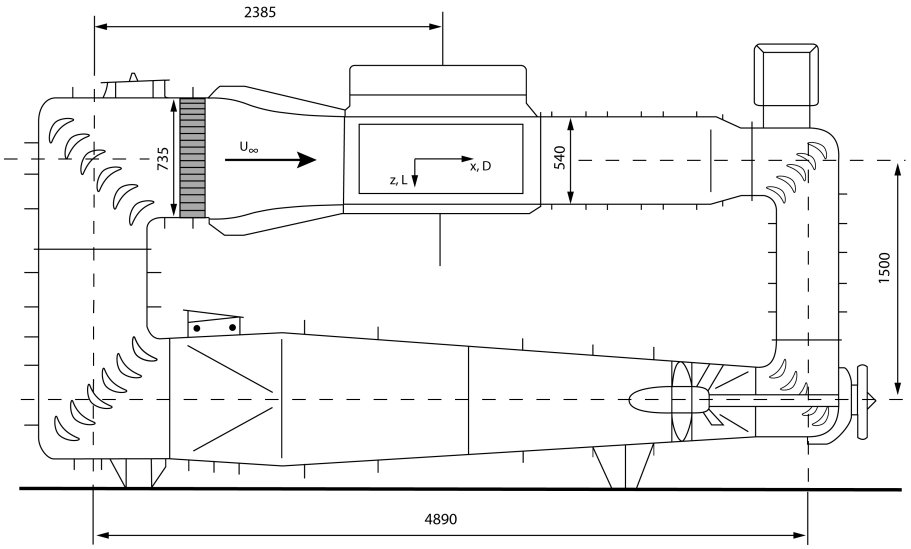

Figure 1 – Sketch of the closed-circuit water tunnel [15].

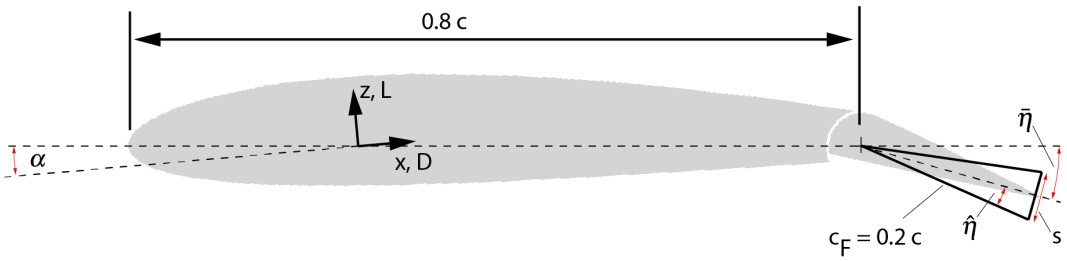

Figure 2 – Geometry and nomenclature of the aerofoil with trailing-edge flap [15].

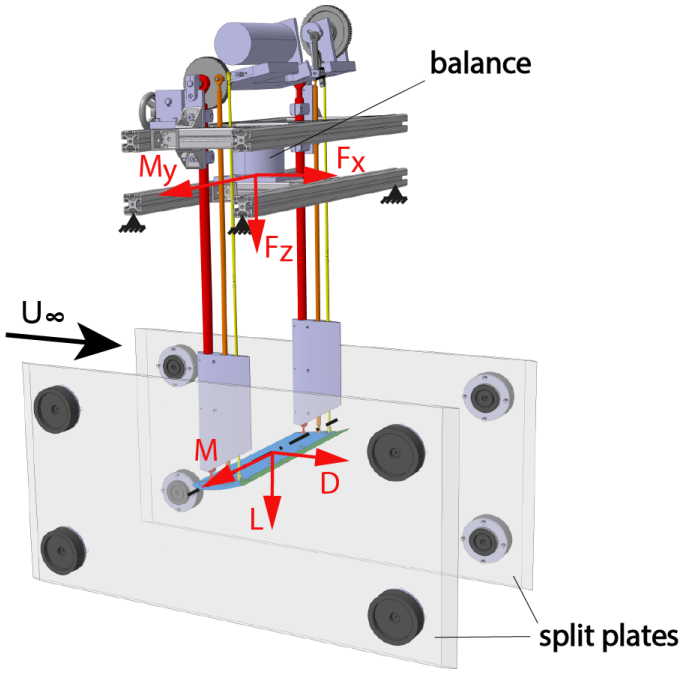

Figure 3 – Experimental setup showing the position of the balance.

In all test cases, the angle of attack of the main wing α is at 5° and the mean flap angle $\bar{\eta}$ is at 16°, beyond this angle, boundary layer separation occurs on the trailing edge. The oscillation amplitude $\hat{\eta}$ is set to four different angles (2°, 4°, 6° and 8°). All parameter are tested at nine reduced frequencies k (0.0025, 0.5, 1.5, 2.5, 3.5, 4.5, 5.5, 6.5 and 7.5), also listed in table 1. The reduced frequency of 0.0025 is used to measure the quasi-steady loads. The reduced frequency is defined as

$$k = \frac{\pi f c}{U_\infty}, \tag{1}$$

where U_∞ is the freestream velocity, f is the oscillation frequency and c is the chord of the aerofoil.

Table 1 – Specifics of the conducted balance measurements.

Hardware and settings		Parameter	
Force balance	ME-Meßsysteme K6D110	angle of attack α	5°
Nominal forces	F_x,F_y =4 kN, F_z =10 kN	mean flap angle $\bar{\eta}$	16°
Nominal moments	M_x,M_y,M_z =250 Nm	oscillation amplitude $\hat{\eta}$	2°, 4°, 6°, 8°
Acquisition unit	GI Q.brixx X station B	reduced frequency k	0.0025
Transducer modules	GI Q.brixx XL A101 (3x)		0.5, 1.5, 2.5, 3.5
Acquisition frequency $f_{s,load}$	20 kHz		4.5, 5.5, 6.5, 7.5

2.4 Particle Image Velocimetry

Triggered Particle Image Velocimetry (triggered PIV) synchronised to the flap frequency is used to capture the phase-averaged flow fields. Figure 4 schematically depicts the used PIV setup. The Nd:Yag laser Quantel Twins Ultra CFR 200 and the optical setup is positioned below the test section spanning a light sheet with a thickness of 2 mm in the test section on mid-span position. The light sheet is in mid-span position to avoid 3D-effects from the wing side wall boundary layer interaction. The field of view (FOV), also depicted in figure 4, shows the vicinity of the trailing-edge flap. The double-frame ccd-camera pco.2000 with a resolution of 2048 x 2048 pixels and a dynamic range of 14 bit is positioned with a 90° angle to the flow direction. The flow is seeded with polyamide particles with a density of 1.183 g/cm^3. The laser pulse separation of the double pulse mode was set to dt = 300 µs, to get a particle shift in the range of 2 to 6 pixels for mean flow velocities.
As well as for the balance measurements, the angle of attack α and the mean flap angle $\bar{\eta}$ are kept constant for the PIV measurements. The experiments with an oscillation amplitude $\hat{\eta}$ of 2° are conducted at three different reduced frequencies k (2.5, 5 and 7.5). The hardware and the parameter of the PIV measurements are listed in table 2.

Table 2 – Specifics of the PIV measurements.

Hardware and settings		Parameter	
Camera	pco.2000, 14 bit CCD	angle of attack α	5°
Lens	Sigma f=28mm, f/8	mean flap angle $\bar{\eta}$	16°
Laser	Quantel Twins Ultra CFR 200	oscillation amplitude $\hat{\eta}$	2°, 4°, 6°, 8°
Wavelength	532 nm (Nd:YAG)	reduced frequency k	2.5, 5, 7.5
Laser pulse separation time	300 µm		
Acquisition frequency $f_{s,PIV}$	1.6 Hz - 2 Hz		
No. of captured flap cycles	300		

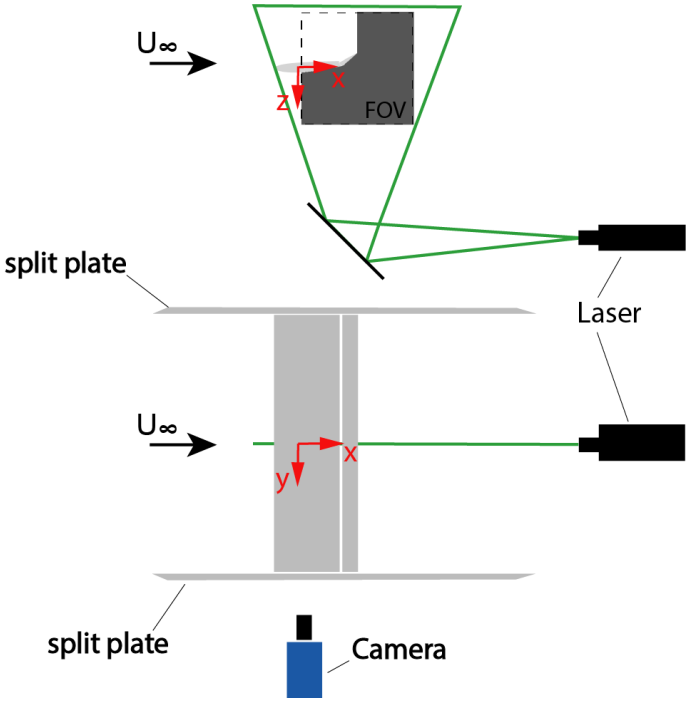

Figure 4 – Sketch of the PIV setup with side view (upper) and top view (lower).

3. Data Processing

3.1 Lift Data

The measured data set from the balance includes among others the force data in z-direction, the flap deflection angle and a time stamp. In order to use the measured signals from the force sensors, post processing is performed with MATLAB. In a first step, the signal runs through a low-pass filter to filter out noise, i.e. the network frequency of the power supply at 50 Hz and vibrations of the flow facility. The cut-off frequency of the low-pass filter is in any case above the flap oscillation frequency f_F. The pass band and stop band cut-off are set individually for any flap oscillation frequency, such that the pass band cut-off frequency is at 1.2 f_F and the stop band cut-off is at 1.4 f_F. In a subsequent processing step, the filtered data is adjusted for gravity forces, drag forces of the wing mount and also transferred from the coordinate system of the balance into the aerodynamic coordinate system. The gravity forces and the aerodynamic drag of the wing mount are subtracted from the total forces measured. After adjusting the data, a processing step follows to truncate the signal. The signal of the flap deflection angle, included in the data, is used to identify the phase angle in order to truncate the signal at the same phase angle at the start and the end. In the last two processing steps, the lift data is time-averaged and phase-averaged.

3.2 Velocity Field Data

The measured PIV data is processed with the software DaVis from LaVision. Two preprocessing steps are made to prepare the particle images. First, a geometric mask is applied to the particle images to exclude the aerofoil and the flap and also the shadow area where the laser light is blocked. Second, a time filter subtracts the average intensity of all images to reduce background noise. The cross-correlation is done in a multi-pass iteration, i.e. four times 96x96 pixels squared interrogation windows followed by four times 24x24 pixels squared interrogation windows. The overlap of the interrogation windows is set to 75%. In the postprocessing, a universal outlier detection and a smoothing over 3x3 pixels is used. In the last processing step, the velocity fields of all flap cycles with the same phase angle are averaged to get the phase-averaged flow fields.

4. Results and Discussion

4.1 Lift of an Oscillating Trailing-Edge Flap

Figure 5 shows the time-averaged lift coefficients as a function of the reduced frequency for the four investigated oscillation amplitudes. The results for all investigated oscillation amplitudes show a lift increase with increasing reduced frequency. The time-averaged lift coefficient of the quasi-steady case with the highest investigated oscillation amplitude $\hat{\eta}$ =8° is the lowest, because boundary layer separation on the trailing edge occurs beyond a flap deflection angle η of 16° (see Figure 8) which is the chosen mean flap angle and hence, the highest oscillation amplitude produces accordingly the strongest separation. However, the disproportionate lift increase becomes apparent for the cases with high amplitude in figure 5. At a reduced frequency k of 4.5, the time-averaged lift coefficients with an oscillation amplitude $\hat{\eta}$ =8° is the highest. The maximum lift coefficient of the investigated cases is 1.57, at an oscillation amplitude of 8° and a reduced frequency k of 6.5. Compared to the quasi-steady case, this is an increase of 71.3%. The maximum lift coefficient for all oscillation amplitudes is reached between a reduced frequency of 5.5 and 6.5. The lift coefficient decreases after reaching its peak value in all cases. To study the lift increase that is most prominent with an oscillation amplitude $\hat{\eta}$ =8°, we take a look at the time history plot of the lift coefficients for the individual investigated reduced frequency values, see figure 6.

Figure 6 shows the time history of the measured lift coefficients of various reduced frequencies with a flap oscillation amplitude $\hat{\eta}$ of 8°. The time t is normalised with the period of a full oscillation cycle T. The quasi-steady case shows a periodic cycle with a minimum at t/T =1 and a maximum at t/T =1.5. With larger unsteadiness, two prominent effects of increasing reduced frequency can be seen. First, a peak of the lift coefficient in the first half of each cycle (downstroke) increases. This is at $t/T = n+0.25$, when the angular flap velocity is highest. Second, another peak in the second half of each cycle (upstroke) is phase shifted. The first effect is due to non-circulatory flow effects, i.e. the added-mass effect, and the second effect is due to circulatory flow effects. The phase shift is clearly visible in the phase-averaged data.

Figure 7 shows the plots of the phase-averaged lift coefficients of nine different reduced frequencies with the same oscillation amplitude of 8°. The downstroke (from lower to higher flap deflection angles) is plotted with a blue line and the upstroke (from higher to lower flap deflection angles) is plotted with a red line. The time-averaged lift coefficient is indicated with a black horizontal line. The highest time-averaged lift coefficient is at k =6.5, as already discussed. As the reduced frequency increases, the unsteady effects also increase and the hysteresis loop widens. With the reduced frequency above 4.5, a second peak in the lift coefficient becomes visible during the downstroke. As the reduced frequency further increases, this peak is phase shifted to lower flap deflection angles in the upstroke cycle and furthermore to higher flap deflection angles in the downstroke cycle. The latter is the case at a reduced frequency of k =7.5.

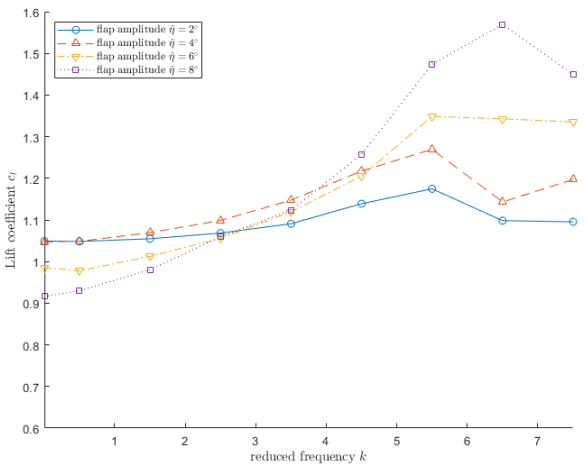

Figure 5 – Time-averaged lift coefficients of a rigid aerofoil with oscillating trailing-edge flap.

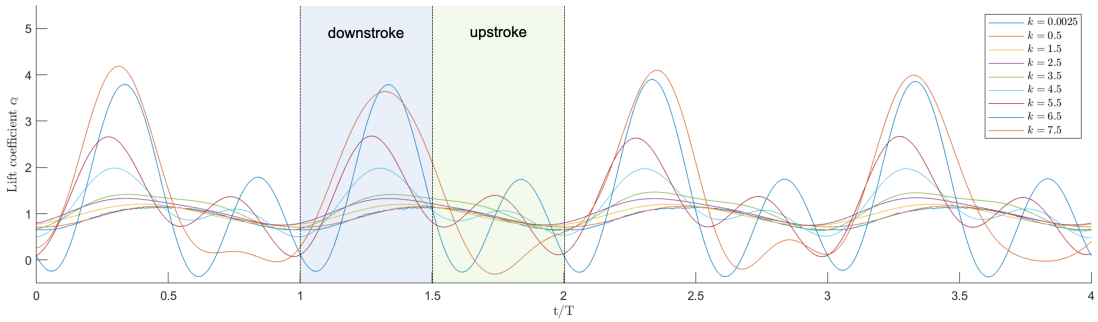

Figure 6 – Time history of lift coefficients with a flap oscillation amplitude of $\hat{\eta}$=8°, showing four cycles of the oscillating trailing-edge flap at nine different reduced frequencies.

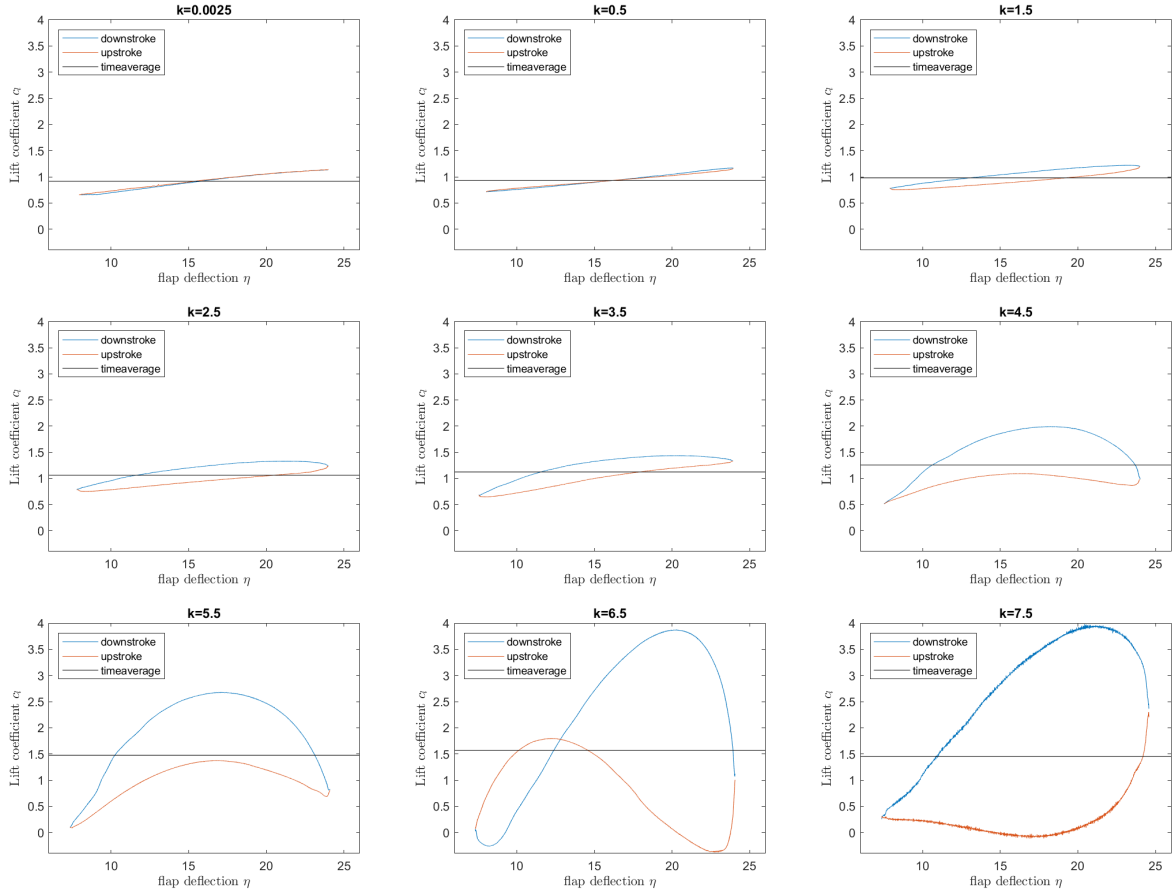

Figure 7 – Phase-averaged lift coefficients for a flap oscillation amplitude of $\hat{\eta}$=8°.

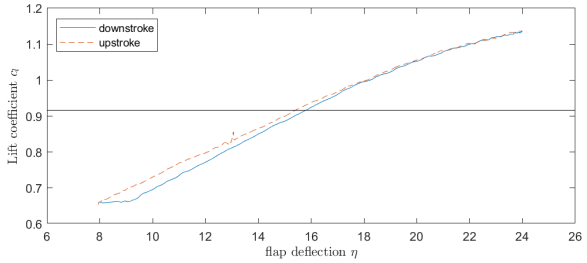

Figure 8 – Phase-averaged lift coefficients for a flap oscillation amplitude of $\hat{\eta}$=8° at k =0.0025.

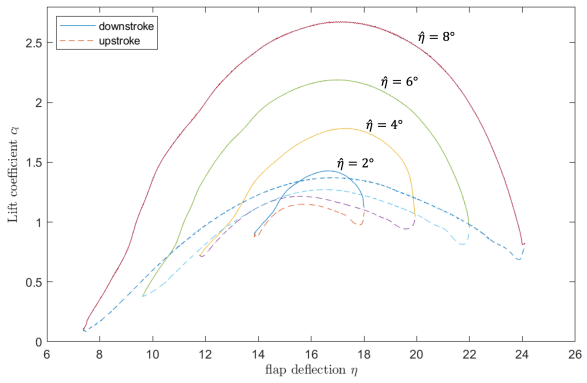

Figure 9 – Phase-averaged lift coefficients for various flap oscillation amplitudes at k =5.5.

To examine the quasi-steady case in more detail, figure 8 shows the phase-averaged lift coefficient at a reduced frequency of 0.0025. The lift coefficient shows a linear increase up to a flap deflection angle of 16°. Because of boundary layer separation occurring beyond this flap deflection angle, the development of the lift coefficient becomes non-linear.
Figure 9 shows the phase-averaged lift coefficients at a reduced frequency of k =5.5, plotted are the results for all oscillation amplitudes. All oscillation amplitudes show qualitatively the same hysteresis. That means the phase shift of the circulatory mechanisms is independent of the oscillation amplitude. It also shows that the added-mass effect is not phase shifted with the oscillation amplitude.

4.2 Vortex Topology in the Wake of an Oscillating Trailing-Edge Flap

Figure 10 depicts the contour plot of the vorticity in the wake flow field. The positive vorticity for anti-clockwise rotation is depicted in red and the negative vorticity for clockwise rotation is depicted in blue. The flap oscillates with an oscillation amplitude of 2° and is shown in all three cases at the maximum deflection angle. The reduced frequency is varied from A) k =2.5, to B) k =5, to C) k =7.5. The vortices that shed at highest angular flap velocity ($t/T = n+0.25$) are indicated in the figure. Keep in mind that the travel distance of the vortices decreases with the frequency because the free stream velocity is constant. It is assumed that the rate of vorticity flux at the trailing edge correlates with rate of change of circulation [17]. Consequently, negative vorticity, i.e. a clockwise rotating vortex sheds, if the lift coefficient increases. In all three reduced frequencies, vortices shed constantly at highest angular flap velocity ($t/T = n+0.25$), i.e. the added-mass vortex. The vortex shedding in between those vortices varies with the reduced frequency. At a reduced frequency of 2.5, another vortex sheds shortly after the added-mass vortex. At a reduced frequency of 5 and 7.5, the vortices in between are phase shifted. Furthermore, with the phase shift at k =7.5 the vortices interact with the added-mass vortex of the following cycle.

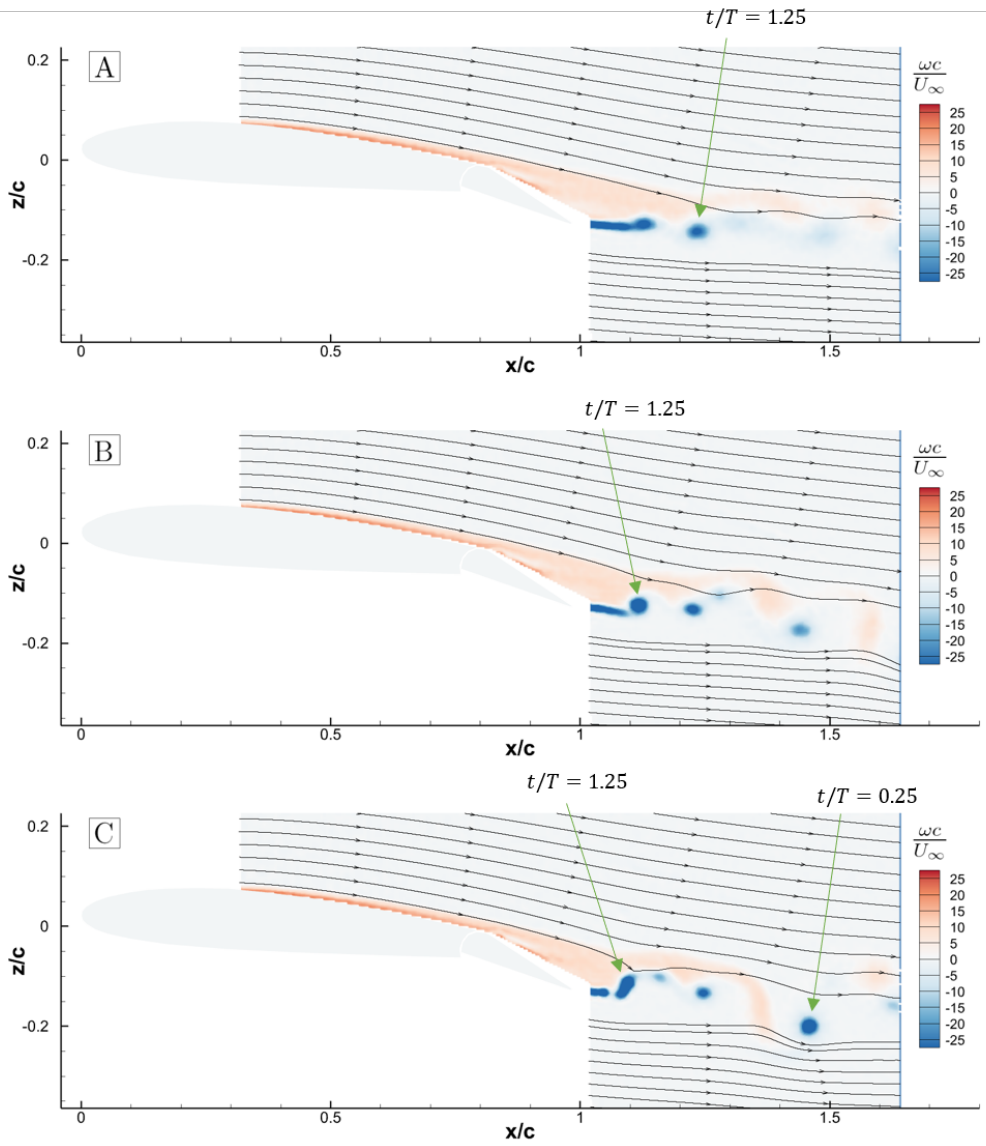

Figure 10 – Contour plot of the vorticity in the flow field in the vicinity of the oscillating trailing-edge flap. The oscillation amplitude of the flap is at $\hat{\eta}$=2° and the reduced frequency is at A) k =2.5, B) k =5 and C) k =7.5. The vortices that shed at highest angular flap velocity ($t/T = n + 0.25$) are indicated.

4.3 Lift-Producing Mechanisms

An oscillating trailing-edge flap has two lift-producing mechanisms, which are described in the literature as circulatory and non-circulatory lift. In a steady flow, the circulatory mechanism is highest at maximum flap deflection angle with attached flow and is equivalent to the bound circulation. In an unsteady flow, the circulatory mechanism is phase shifted, as mentioned in [11] and confirmed by the results of this paper. The mechanism that is not phase shifted and is highest at maximum angular flap velocity can be identified as added-mass effect.
The acceleration of fluid due to the added-mass effect is even more effective, if the flow velocity is low compared to the flap velocity. The lift-producing mechanisms in unsteady flow are non-linear and coupled and therefore superposition cannot be applied. Hence, the average lift of an oscillating trailing-edge flap is at a maximum when the peak of the circulatory mechanism is due to the phase shift in the middle between the peaks of the non-circulatory mechanism. This is the case for reduced frequencies between k =5.5 and k =6.5.

5. Conclusion

In this paper, we present experimental results of a study aiming at characterising the lift-producing mechanisms of an oscillating trailing-edge flap. It is shown that the maximum increase of the lift coefficient is found between k=5.5 and k=6.5 followed by a decrease of the lift coefficient. The concept of non-circulatory and circulatory lift is applied to the measured lift data. The peak in the downstroke is identified as non-circulatory lift, i.e. added-mass effect. The peak frequency in the time-averaged lift coefficients is found between k =5.5 and k =6.5.

6. Acknowledgements

The funding of this investigation within the LuFo V-3 project BIMOD (Influencing maximum lift and wake vortex instabilities by dynamic flap movement) by the German Federal Ministry for Economic Affairs and Climate Action (BMWK), is gratefully acknowledged.

7. Contact Author Email Address

martin.bremm@ilr.rwth-aachen.de

8. Copyright Statement

References

[1] Bernhammer L, Navalkar S, Sodja J, De Breuker R and Karpel M. Experimental and Numerical Investigation of an Autonomous Flap for Load Alleviation. *Journal of Aircraft*, Vol. 54, No. 2, pp 464-475, 2017.

[2] Pohl J, Semaan R and Jones A. Dynamic lift measurements on an airfoil with periodic flap motion at high Reynolds number. *AIAA Scitech 2019 Forum*, San Diego, California, pp 1-16, 2019.

[3] Caruana D, Mignosi A, Corrège M, Le Pourhiet A and Rodde A. Buffet and buffeting control in transonic flow. *Aerospace Science and Technology*, Vol. 9, No. 7, pp 605-616, 2005.

[4] Gao C, Zhang W and Ye Z. Numerical study on closed-loop control of transonic buffet suppression by trailing edge flap. *Computers and Fluids*, Vol. 132, pp 32-45, 2016.

[5] Lee T and Gerontakos P. Dynamic Stall Flow Control via a Trailing-Edge Flap. *AIAA Journal*, Vol. 44, No. 3, pp 469-480, 2006.

[6] Feszty D, Gillies E and Vezza M. Alleviation of airfoil dynamic stall moments via trailing-edge-flap flow control. *AIAA Journal*, Vol. 42, No. 1, pp 17-25, 2004.

[7] Krzysiak A and Narkiewicz J. Aerodynamic Loads on Airfoil with Trailing-Edge Flap Pitching with Different Frequencies. *Journal of Aircraft*, Vol. 43, No. 2, pp 407-418, 2006.

[8] Greenhalgh S. Lift enhancement due to unsteady aerodynamics. *11th Applied Aerodynamics Conference*, Monterey, California, pp 1018-1028, 1993.

[9] Greenhalgh S. Oscillating Flap Lift Enhancement Device. *US. Patent*, No. 5,884,872, 1999.

[10] Stevens P and Babinsky H. Experiments to investigate lift production mechanisms on pitching flat plates. *Experiments in Fluids*, Vol. 58, No. 7, pp 1-17, 2016.

[11] Katz J and Plotkin A. *Low-Speed Aerodynamics*. 2nd edition, Cambridge University Press, 2001.

[12] Leishman J G. Unsteady Lift of a Flapped Airfoil by Indicial Concepts. *Journal of Aircraft*, Vol. 31, No. 2, pp 288-297, 1994.

[13] Shehata H, Zakaria M, Hussein A and Hajj M R. Aerodynamic Analysis of Flapped Airfoil at High Angles of Attack. *2018 AIAA Aerospace Sciences Meeting*, Kissimmee, FL, USA, pp 1-15, 2018.

[14] Shehata H, Zakaria M, Woolsey C and Hajj M. Lift enhancement by a flapped trailing edge at low Reynolds number: A frequency response approach. *Journal of Fluids and Structures*, Vol. 110, No. 103518, pp 1-16, 2022.

[15] Bremm M, Stephan R, Hörnschemeyer R and Stumpf E. Dynamic Trailing-Edge Flap Movement as a Non-Conventional Aerodynamic Lift Mechanism. *32nd Congress of the International Council of the Aeronautical Sciences*, Shanghai, China, pp 1-17, 2021.

[16] Braun S. *Numerische Simulation von Wirbelaufrollvorgängen an Tragflügeln*. Dissertation, RWTH Aachen University, 2016.

[17] Sears W. Some Recent Developments in Airfoil Theory. *Journal of the Aeronautical Sciences*, Vol. 23, No. 5, pp 490-499, 1956.